Cytotoxic T cells specific for alpha-myosin drive immunotherapy related myocarditis

Justin Balko (justin.balko@vumc.org)
Vanderbilt University Medical Center https://orcid.org/0000-0002-4263-5974

Margaret Axelrod
Vanderbilt University Medical Center

Wouter Meijers
Vanderbilt University Medical Center

Elles Screever
Vanderbilt University Medical Center

Mary Grace Carroll
Vanderbilt University Medical Center

Xiaopeng Sun
Vanderbilt University Medical Center

Elie Tannous
Vanderbilt University Medical Center

Juan Qin
Vanderbilt University Medical Center

Yueli Zhang
Vanderbilt University Medical Center

Ayaka Sugiura
Vanderbilt University Medical Center

Jordan Wright
Vanderbilt University Medical Center

Spencer Wei
The University of Texas MD Anderson Cancer Center

Susan Opalenik
Vanderbilt University Medical Center

Abigail Toren
Vanderbilt University Medical Center

Jeffrey Rathmell
jeff.rathmell@vumc.org https://orcid.org/0000-0002-4106-3396

P Ferrell
Vanderbilt University Medical Center https://orcid.org/0000-0003-1140-9154

Elizabeth Phillips

Vanderbilt University https://orcid.org/0000-0002-7623-3383

Simon Mallal

Division of Infectious Diseases, Department of Medicine, Vanderbilt University Medical Center

Douglas Johnson

Vanderbilt University Medical Center https://orcid.org/0000-0002-6390-773X

James Allison

The University of Texas MD Anderson Cancer Center

Javid Moslehi

University of California, San Francisco

Biological Sciences - Article

Keywords:

Posted Date: February 4th, 2022

DOI: https://doi.org/10.21203/rs.3.rs-1315661/v1

Version of Record: A version of this preprint was published at Nature on November 16th, 2022. See the published version at https://doi.org/10.1038/s41586-022-05432-3.

Abstract

Immune-related adverse events, particularly severe toxicities such as myocarditis, are major challenges to immune checkpoint inhibitor (ICI) utility in anti-cancer therapy1. The pathogenesis of ICI-myocarditis is poorly understood. Pdcd1-/-Ctla4+/- mice recapitulate clinicopathologic features of ICI-myocarditis, including myocardial T cell infiltration2. Single cell RNA/T cell receptor (TCR) sequencing on the cardiac immune infiltrate of Pdcd1-/-Ctla4+/- mice identified activated, clonal CD8+ T cells as the dominant cell population. Treatment with anti-CD8, but not anti-CD4, depleting antibodies rescued survival of Pdcd1-/-Ctla4+/- mice. Adoptive transfer of immune cells from mice with myocarditis induced fatal myocarditis in recipients which required CD8+ T cells. Alpha-myosin, a cardiac specific protein absent from the thymus3,4, was identified as the cognate antigen source for three MHC-I restricted TCRs derived from mice with fulminant myocarditis. Peripheral blood T cells from two patients with ICI-myocarditis were expanded by alpha-myosin peptides, and these alpha-myosin expanded T cells shared TCR clonotypes with diseased heart and skeletal muscles, indicating that alpha-myosin may be a clinically important autoantigen in ICI-myocarditis. These studies underscore the critical role for cytotoxic CD8+ T cells, are the first to identify a candidate autoantigen in ICI-myocarditis and yield new insights into ICI toxicity pathogenesis.

Main

Immune checkpoint inhibitors (ICIs) have drastically altered the treatment landscape and prognosis for many cancers. However, not all patients respond to treatment and many patients experience immune-related adverse events (irAEs), especially when ICIs are used in combination. With increasing use of ICIs, preventing, diagnosing, and treating irAEs are urgent clinical challenges. Currently, clinically actionable biomarkers of response and toxicity are limited. Furthermore, the mechanistic basis of irAEs is poorly defined.

Myocarditis is an uncommon irAE, affecting < 1% of ICI-treated patients, but has a mortality rate of nearly 50%[1,5]. Combination ICI therapy (with anti-PD-1 and anti-CTLA4) is the most well-established risk factor for ICI-myocarditis[6–9]. ICI-myocarditis is pathologically characterized by predominance of T lymphocytes and macrophages in the heart and often co-occurs with myositis, with early studies suggesting common clonotypes of T lymphocytes in both tissues[5]. These data suggest the possibility of shared target antigens driving T lymphocyte expansion and activation, which would be critical for pathogenesis; however, experimental data have been lacking.

Generally, mice treated with ICIs do not replicate the full spectrum of irAEs seen in patients, limiting research on mechanisms of toxicity. We have recently described a mouse model of ICI-myocarditis in which C57BL6/J mice with homozygous knockout of *Pdcd1* and heterozygous deletion of *Ctla4* die prematurely and specifically due to myocarditis, recapitulating clinical and pathological features of ICI-myocarditis[2]. Severe inflammation is specific to the heart in these mice. By flow cytometry, the myocardial immune infiltrate is primarily composed of CD8+ T cells, similar to patients with ICI-

myocarditis. Furthermore, treatment with abatacept, a CTLA4 fusion protein, attenuates myocarditis and increases survival in the mice, consistent with early clinical data from patients with ICI-myocarditis treated with abatacept[2,10]. Here we utilize this mouse model of ICI-myocarditis to characterize the immune infiltrates, establish CD8+ T cells as necessary for disease, and identify alpha-myosin as a cognate antigen for the most abundant TCRs in myocarditis. Furthermore, we extend some of these findings into human disease and find that alpha-myosin expanded TCRs are present in inflamed cardiac and skeletal muscles in patients with ICI-myocarditis.

Clonal CD8+ T cells are abundant in ICI-myocarditis

Fulminant myocarditis affects 50% of *Pdcd1-/-Ctla4+/-* mice and is characterized by histologic destruction of the myocardial architecture (Fig. 1a, b)[2]. We used single cell RNA and TCR sequencing to characterize sorted CD45+ infiltrating immune cells from six healthy wild type mouse hearts and four hearts from *Pdcd1-/-Ctla4+/-* mice affected by myocarditis. Dimensionality reduction with uniform manifold approximation and projection (UMAP) and cell type annotation assisted by SingleR reveals distinct clustering by genotype (Fig. 1c; Extended Data Fig. 1a)[11]. Activated T lymphocytes and myeloid cells comprise the majority of the immune cells in myocarditis. The largest difference is seen in the activated T cell cluster, which makes up 34% of the myocarditis immune cells, and only 2% of the control immune cells. Markers of activation such as *Ccl5, Ccl4, Tigit, Nkg7,* and *Gzmb* are upregulated in the T cell clusters in myocarditis compared to control T cell clusters (Fig. 1d). Conversely, markers of naïve status such as *Ccr7, Lef1* and *Sell* are upregulated in control T cells. Activation markers are also upregulated in other clusters, including myeloid cell subsets, in the myocarditis samples (Extended Data Fig. 1b). *Aw112010*, a long noncoding RNA essential for the orchestration of mucosal immunity during infections and in colitis, is strongly upregulated in several clusters in the myocarditis samples[12,13]. In contrast, B lymphocytes make up most of the immune cells in the control heart, consistent with previous studies[14–16].

Given the high infiltration of activated T cells, we next sought to assess the clonality of TCRs in the myocarditis samples using both bulk and single cell TCR sequencing. Cardiac tissue from affected *Pdcd1-/-Ctla4+/-* mice had lower Shannon diversity compared to splenic tissue (whether derived from healthy wild type mice or mice with myocarditis), indicating a higher degree of clonal TCRs (Extended Data Fig. 1c). In single cell TCR data, clonal was defined as more than two cells with the same TCR clonotype (same TCR alpha and beta CDR3 regions). No clonal cells were identified by single cell TCR sequencing of the healthy cardiac immune infiltrate. In contrast, 63% of cells with TCR reads in the myocarditis sample had clonal TCRs and clonal cells were identified in all four myocarditis samples (Extended Data Fig. 1d). Dimensionality reduction of only T cells with TCR reads showed that clonal cells overlap with the activated T cell cluster whereas not clonal cells overlap with naïve T cells (Fig. 1e). A significantly higher proportion of the clonal cells in myocarditis are activated T cells relative to not clonal cells in either control or myocarditis samples (Fig. 1f). Comparing gene expression by clonality shows that not clonal cells from control samples express *Cd8a*, *Cd4*, and markers associated with naïve status,

but not genes associated with activation. In contrast, clonal cells from myocarditis samples express *Cd8a* and cytotoxicity genes such as *Nkg7* and *Gzmb,* but do not express *Cd4* or markers of naïve status (Fig. 1g). These data show that there is a large population of highly activated, clonally expanded CD8+ T cells in murine ICI-myocarditis.

CD8+ T cells are necessary for myocarditis

Using anti-CD8 and anti-CD4 depleting antibodies we tested whether depletion of these cell subsets would attenuate myocarditis and affect survival of *Pdcd1-/-Ctla4+/-* mice. Depletion of target cells was confirmed by flow cytometry on peripheral blood (Extended Data Fig. 2a). Depletion of CD8+ cells, but not CD4+ cells, significantly rescued survival in these mice (Fig. 2a). Conversely, we tested whether transfer of immune cells could recapitulate disease. Adoptive transfer of whole splenocytes, but not splenocytes from which CD8+ cells were depleted, from *Pdcd1-/-Ctla4+/-* mice with myocarditis to *Rag1-/-* recipients was sufficient to induce fatal myocarditis (Fig. 2b). CD8 depletion was confirmed by flow cytometry on transferred splenocytes (Extended Data Fig. 2b). Myocarditis was confirmed histologically on necropsy tissue (Fig. 2c). The single fatality in the CD8 depleted arm was due to a bowel obstruction and there was no evidence of myocarditis histologically. Immunohistochemistry for CD3, CD4, CD8 and F4/80 showed abundant cardiac infiltration of CD3+ and CD8+ cells in the whole splenocyte recipients but not the CD8 depleted recipients. Some CD4+ cells and limited F4/80+ cells were also found in the hearts of whole splenocyte recipients (Fig. 2d; Extended Data Fig. 3a). We performed TCR sequencing on the cardiac tissue of one donor mouse (Donor) and four whole splenocyte recipients (Rec1, Rec2, Rec3, and Rec4; Fig. 2e). High numbers (>2000) of TCR reads were seen in all sequenced hearts, indicating significant T cell infiltration, as expected from histology (Extended Data Fig. 3b). In all four recipient mice the single most clonal TCR beta chain occupied greater than 65% of the total cardiac TCR repertoire, indicating massive expansion of a single TCR clonotype. The most clonal TCR beta chain (CDR3: CASSLRRGEQYF) in the donor heart (which comprised 37% of the donor cardiac repertoire) was expanded in three of four recipients (Rec1, 3, 4). Interestingly, in one recipient mouse (Rec2), a low frequency TCR from the donor was expanded and occupied the majority of the TCR repertoire (CDR3: CASSLGGTVQDTQYF). This high degree of expansion from donor to recipient cardiac tissue suggests a single TCR clonotype may drive myocarditis in the recipient animals. Together, these results strongly indicated that CD8+ T lymphocytes are necessary for the development of myocarditis.

Myocarditis-derived TCRs are specific for alpha-myosin

Next, we aimed to identify the cognate antigen for clonal murine TCRs. TCR-A was derived from the single cell RNA/TCR sequencing and was associated with the activated T cell cluster (Fig. 3a). TCRs B and C were derived from the adoptive transfer of whole splenocytes. TCR-B was the most abundant TCR in the heart of the donor and three recipients (Beta CDR3: CASSLRRGEQYF). TCR-C was the most abundant TCR in the heart of recipient 2 (Beta CDR3: CASSLGGTVQDTQYF; Fig. 2e). CDR3 amino acid sequences, V genes, and J genes are shown in Table 1. These TCRs were reconstructed using Stitchr, cloned and

retrovirally transduced into Jurkat nuclear factor of activated T cells (NFAT)-GFP reporter cells[17–19]. Syngeneic bone marrow derived dendritic cells were used as antigen presenting cells (APCs).

We used a candidate autoantigen approach for TCR screening. Analysis of published RNA sequencing data on thymic APCs (including thymic epithelial cells) showed four cardiac enriched genes (genes where expression in the heart was significantly enriched relative to other tissues) with no detectable expression in the thymus (Fig. 3b)[4]. Lack of thymic expression would be predicted to enable self-reactive T cells to escape negative selection, an important mechanism of tolerance. Of these four genes, *MYH6* (alpha-myosin) has been confirmed by other groups to not be expressed in the thymus in mice or humans and has been shown to be an MHC-II restricted autoantigen in mouse models[3,20,21]. We used a library of 130 overlapping peptides, covering all of alpha-myosin protein (Extended Data Table 1). All three TCR cell lines had NFAT activity in response to alpha-myosin peptides. TCRs A and B activated NFAT reporters in response to the same alpha-myosin peptide ($MYH6_{181-200}$), whereas TCR-C had NFAT activity against a distinct alpha-myosin peptide ($MYH6_{406-425}$; Fig. 3c). From these 20 amino acid peptides, we used TepiTool to narrow down the most likely immunogenic epitopes[22]. TCRs A and B recognize the epitope $MYH6_{191-198}$ (VIQYFASI). TCR-C recognizes the epitope $MYH6_{418-425}$ (VQQVYYSI; Fig. 3d). VIQYFASI and VQQVYYSI both have strong predicted binding to H2-Kb using TepiTool (Extended DataTable 2). The tyrosine and phenylalanine residues at position five of the peptides are known to be key binding epitopes for H2-Kb[23]. In line with these predictions, blocking H2-Kb, but not H2-Db, with an antibody abrogates NFAT reporter activity for all three cell lines (Fig. 3e). All three clonal TCRs derived from independent murine cardiac TCR repertoires recognized alpha-myosin epitopes. Therefore, this strongly suggests that alpha-myosin is an important MHC-I restricted autoantigen in murine ICI-myocarditis.

Alpha-myosin expanded TCRs are present in fulminant myocarditis in patients

We next aimed to test the relevance of alpha-myosin as a potential autoantigen in humans, using three healthy donors and two patients with ICI-myocarditis. ICI-myocarditis patient information is summarized in Table 2. First, we tested whether it was possible to expand alpha-myosin specific T cells from peripheral blood mononuclear cells (PBMCs). PBMCs were stimulated with alpha-myosin peptides or control cytomegalovirus, Epstein-Barr virus and influenza (CEF) peptides (for healthy donors only) for 14 days to generate expanded PBMCs (exPBMC). Shannon diversity decreased significantly from pre-expansion PBMC to alpha-myosin exPBMC for healthy donors and myocarditis patients, indicating clonal expansion of alpha-myosin specific T cells. Interestingly, Shannon diversity did not significantly change from baseline to CEF peptide expansion, suggesting that alpha-myosin is a strong stimulus for clonal T cell expansion (Fig. 4a). For all donors, both alpha-myosin and CEF stimulation resulted in expansion of some individual TCR clonotypes (Extended Data Fig. 4 a, b). These data suggest that both healthy donors and ICI-myocarditis patients have alpha-myosin specific T cells in the periphery that may be expanded.

To assess whether alpha-myosin expanded TCR clones might be involved in cardiac and skeletal muscle toxicity, we compared TCR repertoires in the heart and inflamed muscle to those overrepresented in alpha-myosin exPBMC relative to unexpanded PBMC. We performed bulk TCR sequencing on formalin-fixed

paraffin embedded tissues from endomyocardial biopsy (patient 1 only) and autopsy material (patients 1 and 2). Tissue samples from each myocarditis patient are summarized in Fig. 4b. High numbers of total TCR reads (>1500) were seen in each sequenced sample, consistent with high T cell infiltration (Extended Data Fig. 4c). Shannon diversity was low in heart, diaphragm, and other skeletal muscle samples, indicating clonal TCR repertoires at the sites of toxicity (Fig.4a). Alpha-myosin expanded TCRs (shown in red; count in alpha-myosin exPBMC minus count in pre-expansion PBMC) were present in inflamed tissues from both patients (Fig. 4c; Extended Data Fig. 5a, b). Some alpha-myosin expanded TCRs were present at high frequencies in the inflamed heart and skeletal muscles. This overlap suggests that alpha-myosin may be a relevant disease antigen for ICI-myocarditis and myositis. We performed single cell RNA/TCR sequencing on the sorted CD3+ exPBMC from patient 1 and filtered on only cells with expression of a TCR. Gene expression analysis shows expression of *CD3E* in all cells, presence of both *CD8A* and *CD4* expressing cells, and a very small population of residual *CD79A* expressing B cells (Extended Data Fig. 5c). Clonal cells in the exPBMC are expected to be enriched for alpha-myosin specificity. We further separated cells based on whether their TCR was shared with the cardiac TCR repertoire. Shared TCR clonotypes with the heart would be expected to be enriched for disease relevant TCRs. Following dimensionality reduction with UMAP, the cells cluster distinctly by group (Fig. 4d). Of the cells with TCR clonotypes shared with the heart, a significantly higher proportion were clonal in the exPBMC relative to cells with TCRs not present in the heart (Fig. 4e). Clonal cells with TCRs shared with the diseased heart have high expression of *CD8A* relative to clonal cells with TCRs not present in the heart (Fig. 4f). These data suggest that CD8+ alpha-myosin specific T cells are present at the site of toxicity, in line with results from our mouse model. Clonal cells with TCRs present in the heart also have high expression of markers of activation such as *NKG7*, *GZMB*, and *GNLY* (Fig. 4f). Expression of activation genes in the exPBMC is not expected to reflect *in vivo* cell state, given the two-week *in vitro* expansion period. Rather, higher expression of activation associated genes following stimulation and expansion with alpha-myosin peptides would be expected to further enrich for alpha-myosin specific TCRs and suggest cytotoxic capability of progenitor cells. Taken together, these data suggest that CD8+ cytotoxic T cells specific for alpha-myosin are present in the diseased hearts of patients with fulminant ICI-myocarditis.

Discussion

Immunotherapy toxicities are important limitations to the expanding indications for ICIs. Here we present a new perspective on ICI-myocarditis as an antigen-driven, T cell mediated toxicity. We show in our mouse model that myocarditis is characterized by cytotoxic CD8+ T cells with highly clonal TCRs, and that CD8+ cells are necessary for the development of myocarditis. Three of the most clonal TCRs, derived from independent mice, recognize alpha-myosin epitopes. Two of these TCRs, though derived from independent experiments, recognize the same alpha-myosin epitope. Strikingly, alpha-myosin specific TCRs expanded when transferred to recipient mice and occupied greater than 65% of the highly inflamed cardiac TCR repertoire at the time of death from myocarditis. Lack of thymic expression increases the likelihood that alpha-myosin specific T cells may escape central tolerance mechanisms[3]. Alpha-myosin

specific T cells can be expanded from the blood of healthy donors and patients with ICI-myocarditis. Alpha-myosin expanded TCRs overlap with TCR repertoires in the diseased hearts and skeletal muscle of two patients with fatal ICI-myocarditis. Although presence of shared clones is insufficient to assess whether alpha-myosin specific T cells play a causal role in the initiation of myocarditis, these data suggest that alpha-myosin may be an important autoantigen in ICI-myocarditis. The presence of other high frequency TCRs in the hearts that were not enriched in the alpha-myosin expanded repertoires suggests that there are likely to be other relevant antigens, particularly by the time myocarditis has become severe. Knowledge of the most relevant disease antigens may allow for antigen-directed approaches to suppressing inflammation without sacrificing anti-tumor efficacy such as tolerogenic vaccines. Identification of alpha-myosin as an autoantigen may also permit identification of biomarkers to predict which patients are at higher risk for myocarditis.

Tables

Table 1. Summary of TCR CDR3, V and J genes for murine TCRs used in antigen discovery experiments.

TCR ID	TCR Source	Beta CDR3	TRBV	TRBJ	Alpha CDR3	TRAV	TRAJ	Antigen
A	Single Cell Sequencing	CSAAWGGSAETLYF	TRBV1	TRBJ2-3	CAVSDRGSALGRLHF	TRAV7-3*04	TRAJ18	$MYH6_{191-198}$ (VIQYFASI)
B	Adoptive transfer (Donor, Rec1,3,4)	CASSLRRGEQYF	TRBV15	TRBJ2-7	CALERASGSWQLIF	TRAV13-1	TRAJ22	$MYH6_{191-198}$ (VIQYFASI)
C	Adoptive Transfer (Rec2)	CASSLGGTVQDTQYF	TRBV12-2	TRBJ2-5	CALGDRNNAGAKLTF	TRAV6D-6	TRAJ39	$MYH6_{418-425}$ (VQQVYYSI)

Table 2. Summary of myocarditis patient information.

Patient	Age	Sex	ICI history	Primary Tumor	Disease tissue TCR sequencing
1	75	M	Ipilimumab + Nivolumab	Renal cell carcinoma	Cardiac biopsy; Autopsy: diaphragm, psoas
2	64	M	Nivolumab	Small cell lung cancer	Autopsy: RV, LV, IVS, deltoid, diaphragm

Methods

Mice. Pdcd1-/-Ctla4+/- mice were maintained as previously described[2]. Female mice were used in these studies due to their higher incidence of myocarditis. *Rag1-/-* mice were purchased from The Jackson Laboratory (#002216)[24]. For the generation of survival curves, events were defined as either death (i.e., mice found dead) or identification of mice requiring euthanasia (e.g., due to lethargy, moribund, dyspnea, weight loss). All mice were housed at Vanderbilt University Medical Center vivarium, an Association for Assessment and Accreditation of Laboratory Animal Care International (AAALAC)–accredited, specific pathogen-free (SPF) animal facility. All experiments were performed in accordance with Vanderbilt University Medical Center Institutional Animal Care and Use Committee (IACUC) guidelines.

Preparation of cardiac dissociates for single-cell RNA/TCR sequencing. Single-cell suspensions were obtained from murine hearts by mincing followed by enzymatic digestion with 125 U/mL DNase I (Worthington; cat no. LS002138) and 250 U/mL Collagenase 3 (Worthington; cat no. LS004182). Dissociated hearts were filtered through a 30μm filter. Red blood cells were lysed using ACK lysing buffer (KD Medical/MediaTech; cat no. NC0274127). Single-cell suspensions were either used fresh or cryopreserved in 10% DMSO 90% FBS. Prior to sorting, cells were stained with Alex Flour 488 anti-mouse CD45 (BioLegend; clone 30-F11; cat no. 103122) for 20 minutes at 4°C. Following staining and washing with PBS, cells were resuspended in PBS with DAPI. Live CD45+ immune cells were sorted by fluorescence-activated cell sorting on AF488-positive DAPI-negative events. The wildtype control sample consisted of pooled, without hashing, cardiac immune infiltrates from six female animals, in order to obtain sufficient cells as the healthy heart has a low frequency of cardiac immune cells. The myocarditis sample consisted of four inflamed hearts from female *Pdcd1-/-Ctla4+/-* mice. Inflammation was confirmed by flow cytometry for CD45. Only mice with CD45+ cells comprising greater than ten percent of the total single cells were included. Mice ranged from three to six weeks in age. One inflamed heart was run as an individual sample on the 10X Genomics chromium platform. The additional three inflamed hearts were hashed together using Total Seq C reagents according to the manufacturer's instructions (BioLegend: TotalSeq™-C0301 cat# 155861, TotalSeq™-C0302 cat# 155863, TotalSeq™-C0303 cat# 155865).

Single-cell RNA/TCR sequencing. Each sample (targeting 5,000 – 15,000 cells/sample) was processed for single cell 5' RNA and TCR sequencing utilizing the 10X Chromium system. Libraries were prepared following the manufacturer's protocol. The libraries were sequenced using the NovaSeq 6000 with 150 bp paired end reads. RTA (version 2.4.11; Illumina) was used for base calling and analysis was completed using 10X Genomics Cell Ranger software. Data were analyzed in R using the filtered h5 gene matrices in the Seurat package[25–27]. Briefly, samples were subset to include cells with greater than 200 but less than 3000 unique transcripts to exclude likely non-cellular RNA reads and doublets. Cells with greater than 15% of reads coming from mitochondrial transcripts were also excluded as likely dying cells. For murine hearts, hash tag oligos were deconvoluted using HTODemux with positive quantile set at 0.85. Samples were downsized so that equivalent numbers of cells originating from healthy wild type or myocarditis *Pdcd1-/-Ctla4+/-* cardiac infiltrating immune cells were included (2509 cells per genotype of origin). Ten clusters were identified using a resolution of 0.4. UMAP was used for dimensionality reduction with 15

nearest neighbors and minimum distance of 0.5. Clonal is defined as more than two cells with the same TCR clonotype (defined by unique combinations of CDR3 regions).

T cell receptor sequencing. TCR sequencing and clonality quantification was assessed in formalin-fixed paraffin embedded (FFPE) or snap frozen samples of murine hearts or spleens. All human samples were derived from FFPE or isolated PBMC. For FFPE, RNA was extracted from 10µm sections using the Promega Maxwell 16 FFPE RNA kits and the manufacturer's protocol. TCRs were sequenced using the TCR Immunoverse all chain assay following the manufacturer's protocol (Invitae/ArcherDX). Sequencing results were evaluated using the Archer Immunoverse analyzer. CDR3 sequences and frequency tables were extracted from the manufacturers' analysis platform and imported into R for analysis using the Immunarch package (https://immunarch.com) in R.

Antibody-mediated depletion. Female *Pdcd1-/-Ctla4+/-* mice were randomly assigned to control, anti-CD8a, or anti-CD4 injections at 21 days of age. Mice were injected intraperitoneally three times a week with 200µg of anti-CD4 (BioXCell, Cat# BE0003-1, clone GK1.5) or anti-CD8 (BioXCell, Cat# BE0061, clone 2.43) depleting antibodies or vehicle, all in a maximum volume of 100µL. Treatment lasted until 90 days of age. Peripheral blood was sampled via tail prick for assessment of depletion efficiency at week 3.

Adoptive transfer. Splenocytes were isolated from *Pdcd1-/-Ctla4+/-* mice with myocarditis by manual dissociation, filtering, and red blood cell lysis. Myocarditis of the donor mice was confirmed by either H&E or dissociation of the heart and flow cytometry for CD45+ immune cells. A portion of each spleen underwent CD8 depletion using magnetic bead isolation (Miltenyi CD8 (TIL) MicroBeads, Mouse, Cat# 130-116-478). One million whole or CD8 depleted splenocytes were injected into each *Rag1-/-* recipient mouse in 100µL PBS via tail vein injection. Mice were monitored for death or signs of distress. At death or euthanasia, hearts, spleens, livers, lungs, and kidneys were stained by H&E and evaluated microscopically.

Histology and pathology. Formalin-fixed tissues were processed routinely into paraffin blocks, sectioned at 5µm, and stained with H&E by standard protocols in Vanderbilt University Medical Center's Translational Pathology Shared Resource (TPSR) core laboratory. To further characterize the mononuclear cardiac infiltrates detected by light microscopy, a panel of IHC markers was employed. IHC staining was performed in the TPSR using standard, validated protocols for chromogenic IHC. All steps besides dehydration, clearing, and coverslipping were performed on the Leica Bond-Max IHC autostainer (Leica Biosystems Inc.). Slides were deparaffinized. Antigen retrieval was performed using EDTA (CD markers) or proteinase K (F4/80). Slides were incubated with primary antibodies as indicated below. Secondary antibody labeling was performed for all markers except CD3 by incubating in rabbit anti-rat antibody (BA-4001, Vector Laboratories, Inc.) for 15 minutes at a 1:650 dilution. Immunolabeling by rabbit antibody was visualized using the Bond polymer refine detection system (#DS9800, Leica Biosystems, Inc.). Slides were then dehydrated, cleared, and coverslipped. For primary antibodies, anti-CD3 (Abcam, Ab16669) was used at 1:250 dilution, anti-CD4 (eBioscience, 14–9766–82) was used at 1:1,000 dilution,

anti-CD8 (eBioscience, 14–0808–82) was used at 1:1,000 dilution, and anti-F4/80 (Novus Biologicals, NB600–404) was used at 1:900 dilution.

Flow cytometry. Samples were run on an Attune NxT Acoustic Focusing Cytometer (Life Technologies). Analysis was performed in FlowJo. Gating was first done on forward scatter and side scatter to exclude debris. Doublets were excluded by gating on FSC area versus FSC height. DAPI was used to exclude dead cells from analyses. Antibodies used: CD45-PerCP/Cy5.5 (BioLegend, cat# 103132, clone 30-F11), CD3-AF488 (BioLegend, cat# 100210, clone 17A2), CD4-APC (BioLegend, cat# 100412, clone GK1.5), CD8a-PE/Cy7 (BioLegend, cat# 100722, clone 53-6.7), Thy1.1 (BioLegend, cat# 202506, Clone OX-7) and TCR-beta chain (BioLegend, cat# 109208, Clone H57-597).

TCR sequences and cloning. TCR sequences were generated from CDR3 regions, V genes and J genes using Stitchr[17]. Alpha genes and beta genes were separated using a T2A sequence. Restriction digest sites were added to either end. Full TCR gene blocks were synthesized as custom orders from Genewiz. Full TCR block sequences can be found in supplemental material. TCR sequences were cloned into MSCV-IRES-Thy1.1 DEST vector. MSCV-IRES-Thy1.1 DEST was a gift from Anjana Rao (Addgene plasmid # 17442; http://n2t.net/addgene:17442 ; RRID:Addgene_17442)[28]. Retrovirus was made using the platA retroviral packaging cell line (Cell BioLabs RV-102). Jurkat-TCR-ko-CD8+-NFAT-GFP reporter cells were a gift from Dr. Peter Steinberger. Reporter cells were retrovirally transduced with TCRs of interest. TCR expression was confirmed via flow cytometry for Thy1.1 and TCR-beta chain. Retrovirally transduced cells were sorted on the WOLF cell sorter (NanoCellect) for Thy1.1-AF488. Cells were confirmed to be >90% Thy1.1 positive post-sort prior to use in downstream assays.

Antigen discovery. Jurkat-NFAT-GFP cell lines with reconstructed TCRs were used for antigen screening. Syngeneic (derived from C57BL6 mice) bone marrow derived dendritic cells (BMDCs) were used as APCs. BMDCs were generated by flushing femurs and tibias from mice with PBS, filtering the cells though a 70μM filter, lysing RBCs, and plating in RMPI + 10% FBS + 1% HEPES + 20ng/mL GM-CSF (ProSpec Cat# CYT-222). BMDCs were polarized in GM-CSF containing media for 9 days (replacing the media at days 3 and 6) prior to harvesting the adherent fraction via mechanical dissociation using a cell scrapper and cryopreservation for future experiments. For antigen discovery, BMDCs were thawed into GM-CSF containing media in flat bottom plates the day before adding TCR cell lines and peptides. Cells were plated at a ratio of 1 TCR cell to 3 BMDCs. The alpha myosin peptide library was generated as 20aa peptides with 5aa overlaps from GenScript. Due to insolubility in aqueous solution, two 20aa peptides were replaced by three 10aa peptides each. Sequences of all 130 alpha-myosin peptides are shown in Extended Data Table 1. Peptides were added at a concentration of 10μg/mL and co-cultures were incubated overnight. TCR cell lines were stained with DAPI to assess viability and analyzed via flow cytometry for NFAT-GFP reporter activity.

MHC blocking. Jurkat TCR cell lines were co-cultured with EL-4 cells as APCs with or without 10μg/mL cognate peptide overnight. EL-4 cells were a gift from Dr. Simon Mallal. Blocking antibodies (anti-Db clone 28-14-8S or anti-Kb clone B8-24-3) were added to cells at a concentration of 10μg/mL for 1 hour

prior to adding peptides. Blocking antibodies were generously provided by Dr. John Sidney. TCR cell lines were stained with Thy1.1-APC/Cy7 (BioLegend, cat# 202506, Clone OX-7) to differentiate from EL-4s and with DAPI to assess viability and analyzed via flow cytometry for NFAT-GFP reporter activity.

Patients. Healthy donors provided informed consent under an institutionally approved protocol (IRB# 030062). Myocarditis patients and families provided informed consent for research use of biospecimens and clinical data (IRB# 191213).

Generation of LCLs from PBMC. EBV-transformed lymphoblastoid B cell lines were generated from cryopreserved donor PBMCs by infection with EBV virus stock[29,30]. Approximately, 1-3 × 10^6 PBMCs in RPMI-1640 media supplemented with non-heat inactivated 20% fetal bovine serum (FBS), 1 µg/mL cyclosporin A (CSA; Sigma-Aldrich C1832), and 2.5 µg/mL CpG (Invitrogen ODN2006) were infected with filtered EBV stock and cultured for 2-3 weeks, until clusters of cells were visible by light microscopy.

PBMC expansion. PBMCs were isolated from EDTA collection tubes and processed using a Ficoll gradient. Antigen-specific PBMC expansion was adapted from previously described protocols[31,32]. Fresh or cryopreserved PBMCs were stimulated with 130 pooled alpha-myosin peptides at a final concentration of 400ng/mL of each peptide or a pool of control CMV, EBV, and flu (CEF) peptides (AnaSpec, AS-61036-003). PBMCs were cultured in CTS OpTmizer medium (CTS OpTmizer T Cell Expansion SFM with CTS supplement A1048501, substituted with 2mM L-glutamine, and 2% human serum, Sigma-Aldrich, H3667) with cytokine supplementation (25ng/mL each of rhIL-2, rhIL-7 and rhIL-15, Peprotech). For myocarditis patients 1 and 2, expansion cultures were also supplemented with autologous LCLs to serve as antigen presenting cells at a ratio of 1 APC per 10 PBMC. For healthy donors, expansion was done directly from fresh, not cryopreserved, blood. Peptides were only added on the first day of culture. On day 3, additional media with cytokines was added. On day 7, cells were transferred to a new culture dish with fresh media with cytokines. Cells were analyzed or cryopreserved on day 14.

Single cell sequencing of exPBMC. Expanded PBMCs (exPBMC) from patient 1 were prepared for single cell sequencing as follows. exPBMC were incubated with Human TruStain FcX™ (Fc Receptor Blocking Solution; BioLegend cat# 422302) for 5 minutes on ice, then washed and incubated with human anti-CD3-AF488 (BioLegend, cat# 300319, clone HIT3a) for 30 minutes on ice, and then washed and resuspended to a concentration of 5x10^5 cells/mL. SYTOX AADvanced™ Ready Flow™ Reagent (Invitrogen, cat# R37173) was used following the manufacturer's instructions to exclude dead cells. CD3+ live cells were sorted on the WOLF cell sorter (Nanocellect). Cells were sequenced and data were analyzed as described above. Data were analyzed in R using the filtered h5 gene matrices in the Seurat package[25–27]. Briefly, samples were subset to include cells with greater than 200 but less than 4000 unique transcripts to exclude likely non-cellular RNA reads and doublets. Cells with greater than 15% of reads coming from mitochondrial transcripts were also excluded as likely dying cells. Clonal is defined as more than two cells with the same TCR clonotype (defined by unique combinations of CDR3 regions). For exPBMC, 5,816 cells with TCR reads were analyzed. To identify TCRs overlapping with the cardiac repertoire, beta CDR3 sequences were used.

Statistical analysis. All statistical analyses were performed in R. All single-cell statistical analyses were calculated in R using the Seurat package[25–27]. Visualization and graph generation was performed in R. Shannon diversity was calculated using the R package vegan[33]. The R package immunarch was used for evaluating TCR repertoires[34]. P-value cut-offs displayed on plots correspond to “ns” equals p>0.05, * equals 0.01<p< 0.05, ** equals 0.001<p<0.01, *** equals 0.0001<p<0.001, **** equals p<0.0001.

Data Availability. All data will be made available upon reasonable request to J.M.B.

Declarations

Acknowledgements

We thank the patients and families who donated tissue to this study. We thank M. Madden and M. Korrer for assistance with sample acquisition. We thank members of the J.M.B. laboratory and B.I. Reinfeld for their constructive input. We thank S. Mallal, P. Steinberger and J. Sidney for cell lines and reagents. This work was supported by F30CA236157, T32GM007347 (MLA), R01HL141466(JM), R01HL155990 (JM), R01CA227481(DBJ, JMB), R01HL156021 (JMB, JJM), P30 AI110527 (SM), Susan and Luke Simons Directorship in Melanoma, Van Stephenson Melanoma Research Fund, and James C. Bradford Melanoma Fund (DBJ). W. Meijers is supported by the Mandema-Stipendium of the Junior Scientific Masterclass 2020- 10 of the University Medical Center Groningen and by the Dutch Heart Foundation (Dekker grant 03-005-2021-T005). JP Allison is a CPRIT Distinguished Scholar in Cancer Research. We acknowledge the Translational Pathology Shared Resource supported by NCI/NIH Cancer Center Support Grant 5P30 CA68485-19 and the Shared Instrumentation Grant S10 OD023475-01A1 for the Leica Bond RX. The Vanderbilt VANTAGE Core, including A. Jones and L. Raju, provided technical assistance for this work. VANTAGE is supported in part by a CTSA Grant (5UL1 RR024975-03), the Vanderbilt Ingram Cancer Center (P30 CA68485), the Vanderbilt Vision Center (P30 EY08126) and the NIH/NCRR (G20 RR030956). Figures 1a and 4b were created with BioRender.com.

Conflict of Interest Disclosure

M.L. Axelrod is listed as a coinventor on a provisional patent application for methods to predict therapeutic outcomes using blood-based gene expression patterns, that is owned by Vanderbilt University Medical Center, and is currently unlicensed. S.C. Wei is an employee of Spotlight Therapeutics, a consultant for BioEntre, and an inventor on a patent for a genetic mouse model of autoimmune adverse events and immune checkpoint blockade therapy (PCT/US2019/050551) pending to Board of Regents, The University of Texas System. J.C. Rathmell is a founder, scientific advisory board member, and stockholder of Sitryx Therapeutics, a scientific advisory board member and stockholder of Caribou Biosciences, a member of the scientific advisory board of Nirogy Therapeutics, has consulted for Merck, Pfizer, and Mitobridge within the past three years, and has received research support from Incyte Corp., Calithera Biosciences, and Tempest Therapeutics. P.B. Ferrell receives research support from Incyte Corporation. D.B.Johnson has served on advisory boards or as a consultant for BMS, Catalyst

Biopharma, Iovance, Jansen, Mallinckrodt, Merck, Mosaic ImmunoEngineering, Novartis, Oncosec, Pfizer, and Targovax, has received research funding from BMS and Incyte, and has patents pending for use of MHC-II as a biomarker for immune checkpoint inhibitor response, and abatacept as treatment for immune-related adverse events. J.P. Allison reports personal fees from Achelois, Adaptive Biotechnologies, personal fees from Apricity Health, personal fees from BioAtla, Candel Therapeutics, personal fees from Codiak BioSciences, personal fees from Dragonfly Therapeutics, Earli, Enable Medicine, personal fees from Hummingbird, personal fees from ImaginAb, personal fees from Jounce Therapeutics, personal fees from Lava Therapeutics, personal fees from Lytix Biopharma, personal fees from Marker Therapeutics, PBM Capital, Phenomic AI, personal fees from BioNTech, and personal fees from Polaris Pharma, Time Bioventures, Trained Therapeutics, Two Bear Capital, Venn Biosciences outside the submitted work; in addition, J.P. Allison has a patent for a genetic mouse model of immune checkpoint blockade induced immune-related adverse events pending to The University of Texas MD Anderson Cancer Center; and have received royalties from intellectual property licensed to BMS and Merck. J. Moslehi has served on advisory boards for Bristol Myers Squibb, Takeda, Audentes, Deciphera, Janssen, Immuno-Core, Boston Biomedical, Amgen, Myovant, Kurome Therapeutics, Star Therapeutics, ProtinQure, Pharmacyclics, Pfizer, Mallinckrodt Pharmaceuticals, Silverback Therapeutics, Cytokinetics, and AstraZeneca. J. M. Balko receives research support from Genentech/Roche, and Incyte Corporation, and is an inventor on provisional patents regarding immunotherapy targets and biomarkers in cancer. No disclosures were reported by the other authors.

Author Contributions

M.L.A., J.J.M. and J.M.B. conceived and designed the study and composed the manuscript. W.C.M., E.M.S., E.T., J.Q. and Y.Z. managed the mouse colony and identified appropriate animals for each experiment. M.L.A., W.C.M., E.M.S., M.G.C., X.S., J.J.W., E.T., J.Q. and A.L.T. performed mouse necropsies, tissue dissociation and cryopreservation. M.L.A. performed single cell RNA/TCR and bulk TCR data analyses and figure generation. M.L.A., A.L.T., and X.S. prepared samples for single cell sequencing. W.C.M. and E.M.S. performed antibody mediated depletion studies. A.S. provided expertise and performed tail vein injections for adoptive transfer studies. M.L.A. and M.G.C. performed antigen discovery, epitope identification, and MHC blocking experiments. S.C.W. and J.P.A. provided expertise regarding the mouse model and myocarditis phenotype. S.R.O. provided technical expertise in experimental design and manuscript editing. J.C.R. provided immunology expertise. P.B.F. provided expertise regarding single cell studies. E.J.P. and S.M. provided expertise in experimental design regarding LCLs, antigen discovery, and MHC blocking. D.B.J. and J.J.M. provided clinical expertise, assistance acquiring human samples for this study, and assistance with manuscript writing. M.L.A. analyzed all data generated in this study. J.M.B. obtained funding for this study.

References

1. Wang DY, Salem J-EE, Cohen J V., et al. Fatal Toxic Effects Associated With Immune Checkpoint Inhibitors: A Systematic Review and Meta-analysis. *JAMA Oncol*. 2018;4(12):1721-1728.

http://www.embase.com/search/results?subaction=viewrecord&from=export&id=L624011231. Accessed October 15, 2019.

2. Wei SC, Meijers WC, Axelrod ML, et al. A Genetic Mouse Model Recapitulates Immune Checkpoint Inhibitor–Associated Myocarditis and Supports a Mechanism-Based Therapeutic Intervention. *Cancer Discov*. 2020;11(3):614-639. doi:10.1158/2159-8290.cd-20-0856

3. Lv H, Havari E, Pinto S, et al. Impaired thymic tolerance to α-myosin directs autoimmunity to the heart in mice and humans. *J Clin Invest*. 2011;121(4):1561-1573. doi:10.1172/JCI44583

4. Gabrielsen ISM, Helgeland H, Akselsen H, et al. Transcriptomes of antigen presenting cells in human thymus. *PLoS One*. 2019;14(7):e0218858. doi:10.1371/JOURNAL.PONE.0218858

5. Johnson DB, Balko JM, Compton ML, et al. Fulminant myocarditis with combination immune checkpoint blockade. *N Engl J Med*. 2016;375(18):1749-1755. doi:10.1056/NEJMoa1609214

6. Hu J-RR, Florido R, Lipson EJ, et al. Cardiovascular toxicities associated with immune checkpoint inhibitors. *Cardiovasc Res*. 2019;115(5):854. https://academic.oup.com/cardiovascres/advance-article/doi/10.1093/cvr/cvz026/5304411. Accessed March 4, 2019.

7. Salem JE, Manouchehri A, Moey M, et al. Spectrum of cardiovascular toxicities of immune checkpoint inhibitors: A pharmacovigilance study. *Lancet Oncol*. 2018;19(12):1579. doi:10.1016/S1470-2045(18)30608-9

8. Moslehi J, Lichtman AH, Sharpe AH, Galluzzi L, Kitsis RN. Immune checkpoint inhibitor–associated myocarditis: manifestations and mechanisms. *J Clin Invest*. 2021;131(5). doi:10.1172/JCI145186

9. Zamami Y, Niimura T, Okada N, et al. Factors Associated With Immune Checkpoint Inhibitor–Related Myocarditis. *JAMA Oncol*. 2019;5(11):1635-1637. doi:10.1001/JAMAONCOL.2019.3113

10. Salem J-E, Allenbach Y, Vozy A, et al. Abatacept for Severe Immune Checkpoint Inhibitor–Associated Myocarditis. *N Engl J Med*. 2019;380(24):2377-2379. doi:10.1056/NEJMc1901677

11. Aran D, Looney AP, Liu L, et al. Reference-based analysis of lung single-cell sequencing reveals a transitional profibrotic macrophage. 2019;20(2):163-172. doi:10.1038/s41590-018-0276-y

12. Yang X, Bam M, Becker W, Nagarkatti PS, Nagarkatti M. Long Noncoding RNA AW112010 Promotes the Differentiation of Inflammatory T Cells by Suppressing IL-10 Expression through Histone Demethylation. *J Immunol*. 2020;205(4):987-993. doi:10.4049/jimmunol.2000330

13. Jackson R, Kroehling L, Khitun A, et al. *The Translation of Non-Canonical Open Reading Frames Controls Mucosal Immunity*. Vol 564. Nature Publishing Group; 2018:434-438. doi:10.1038/s41586-018-0794-7

14. Adamo L, Rocha-Resende C, Lin CY, et al. Myocardial B cells are a subset of circulating lymphocytes with delayed transit through the heart. *JCI insight*. 2020;5(3). doi:10.1172/JCI.INSIGHT.134700

15. Bönner F, Borg N, Burghoff S, Schrader J. Resident cardiac immune cells and expression of the ectonucleotidase enzymes CD39 and CD73 after ischemic injury. *PLoS One*. 2012;7(4). doi:10.1371/JOURNAL.PONE.0034730

16. Martini E, Kunderfranco P, Peano C, et al. Single-Cell Sequencing of Mouse Heart Immune Infiltrate in Pressure Overload-Driven Heart Failure Reveals Extent of Immune Activation. *Circulation*. 2019;140(25):2089-2107. doi:10.1161/CIRCULATIONAHA.119.041694

17. Heather JM, Spindler MJ, Alonso MH, et al. Stitchr: stitching coding TCR nucleotide sequences from V/J/CDR3 information. *bioRxiv*. December 2021:2021.12.20.473544. doi:10.1101/2021.12.20.473544

18. Rosskopf S, Leitner J, Paster W, et al. A Jurkat 76 based triple parameter reporter system to evaluate TCR functions and adoptive T cell strategies. *Oncotarget*. 2018;9(25):17608-17619. doi:10.18632/oncotarget.24807

19. Jutz S, Leitner J, Schmetterer K, et al. Assessment of costimulation and coinhibition in a triple parameter T cell reporter line: Simultaneous measurement of NF-κB, NFAT and AP-1. *J Immunol Methods*. 2016;430:10-20. doi:10.1016/j.jim.2016.01.007

20. Gil-Cruz C, Perez-Shibayama C, de Martin A, et al. Microbiota-derived peptide mimics drive lethal inflammatory cardiomyopathy. *Science (80-)*. 2019;366(6467):881-886. doi:10.1126/science.aav3487

21. Massilamany C, Gangaplara A, Steffen D, Reddy J. Identification of novel mimicry epitopes for cardiac myosin heavy chain-α that induce autoimmune myocarditis in A/J mice. *Cell Immunol*. 2011;271(2):438-449. doi:10.1016/J.CELLIMM.2011.08.013

22. Paul S, Sidney J, Sette A, Peters B. TepiTool: A pipeline for computational prediction of T cell epitope candidates. *Curr Protoc Immunol*. 2016;2016:18.19.1-18.19.24. doi:10.1002/cpim.12

23. Falk K, Rotzschke O, Stevanovic S, Jung G, Rammenseet H-G. Allele-specific motifs revealed by sequencing of self-peptides eluted from MHC molecules. 1991.

24. Mombaerts P, Iacomini J, Johnson RS, Herrup K, Tonegawa S, Papaioannou VE. RAG-1-deficient mice have no mature B and T lymphocytes. *Cell*. 1992;68(5):869-877. doi:10.1016/0092-8674(92)90030-G

25. Satija R, Farrell JA, Gennert D, Schier AF, Regev A. Spatial reconstruction of single-cell gene expression data. 2015;33(5):495-502. doi:10.1038/nbt.3192

26. Butler A, Hoffman P, Smibert P, Papalexi E, Satija R. Integrating single-cell transcriptomic data across different conditions, technologies, and species. *Nat Biotechnol*. 2018;36(5):411-420.

doi:10.1038/nbt.4096

27. Stuart T, Butler A, Hoffman P, et al. Comprehensive Integration of Single-Cell Data. *Cell*. 2019;177(7):1888-1902.e21. doi:10.1016/j.cell.2019.05.031

28. Wu Y, Borde M, Heissmeyer V, et al. FOXP3 controls regulatory T cell function through cooperation with NFAT. *Cell*. 2006;126(2):375-387. doi:10.1016/J.CELL.2006.05.042

29. Oh HM, Oh JM, Choi SC, et al. An efficient method for the rapid establishment of Epstein-Barr virus immortalization of human B lymphocytes. *Cell Prolif*. 2003;36(4):191-197. doi:10.1046/J.1365-2184.2003.00276.X

30. Granato M, Santarelli R, Farina A, et al. Epstein-Barr Virus Blocks the Autophagic Flux and Appropriates the Autophagic Machinery To Enhance Viral Replication. *J Virol*. 2014;88(21):12715. doi:10.1128/JVI.02199-14

31. Wölfl M, Greenberg PD. Antigen-specific activation and cytokine-facilitated expansion of naive, human CD8+ T cells. *Nat Protoc 2014 94*. 2014;9(4):950-966. doi:10.1038/nprot.2014.064

32. Eberhardt CS, Kissick HT, Patel MR, et al. Functional HPV-specific PD-1+ stem-like CD8 T cells in head and neck cancer. *Nat 2021 5977875*. 2021;597(7875):279-284. doi:10.1038/s41586-021-03862-z

33. Oksanen J, Blanchet FG, Friendly M, et al. Package “vegan” Title Community Ecology Package Version 2.5-7. 2020.

34. Nazarov V, immunarch.bot, Rumynskiy E. immunarch: An R Package for Painless Bioinformatics Analysis of T-Cell and B-Cell Immune Repertoires. June 2020. doi:10.5281/ZENODO.3893991

Figures

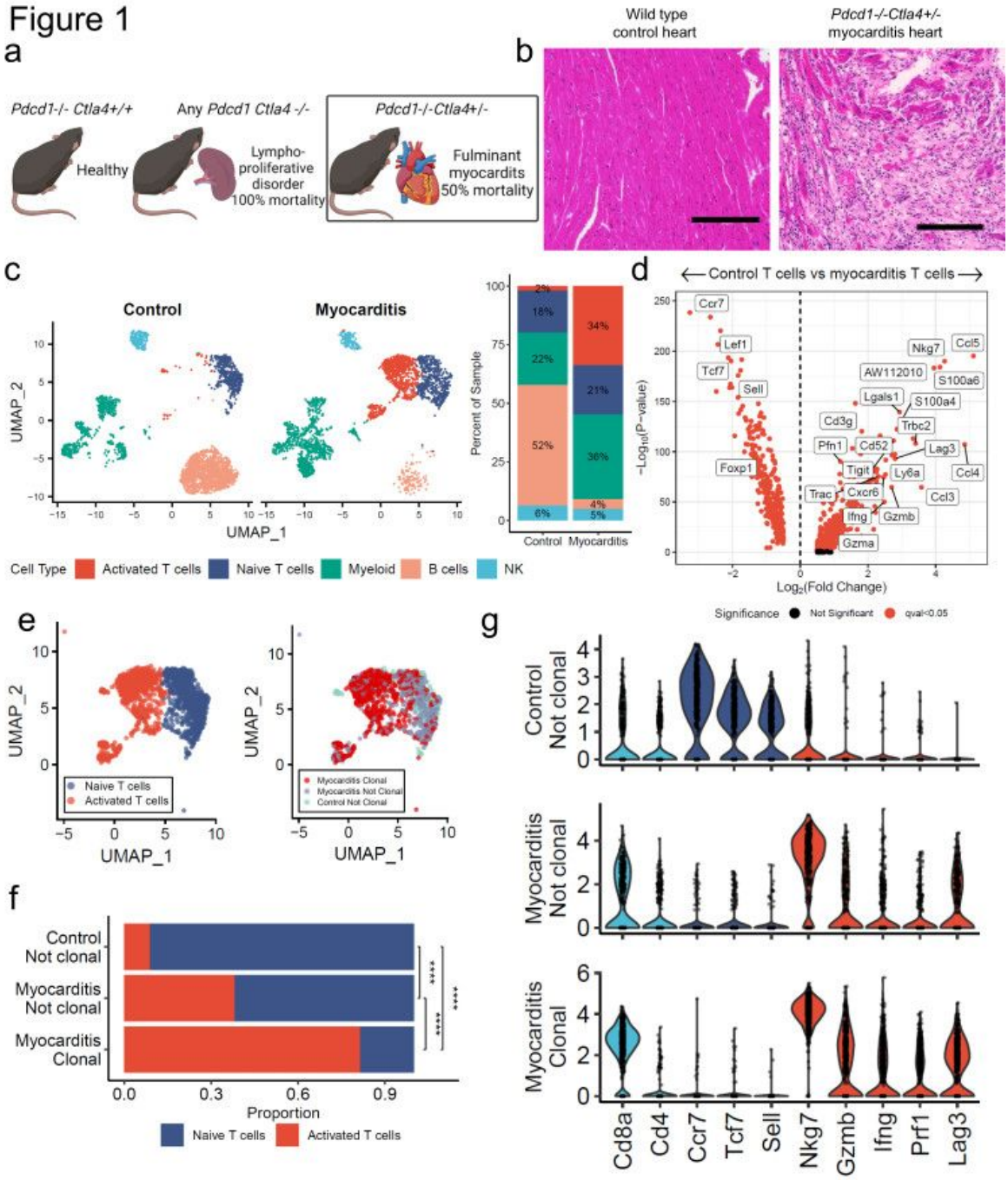

Figure 1

Single Cell RNA/TCR sequencing reveals abundant highly activated, clonal CD8+ T cells in ICI-myocarditis. a) Phenotypic summary of mice with different combinations of *Pdcd1* and *Ctla4* genetic loss. *Pdcd1-/-Ctla4+/+* mice do not have an overt phenotype. Mice with complete loss of *Ctla4* have a fatal lymphoproliferative disorder, regardless of *Pdcd1* genotype. *Pdcd1-/-Ctla4+/-* mice develop fulminant myocarditis and are the focus of this study. b) H&E of cardiac tissue from a healthy wild type

mouse and a *Pdcd1-/-Ctla4+/-* mouse with myocarditis. Scale bar represents 200μm. c) Dimensionality reduction with UMAP of single cell RNA sequencing on sorted CD45+ immune cells from control wild type mouse hearts (n=6) compared to hearts (n=4) of *Pdcd1-/-Ctla4+/-* mice with myocarditis (n= 2509 cells per genotype of origin). Cell type annotations were assisted by singleR and are quantified on the right. d) Differential gene expression between control and myocarditis T cells (both activated and naïve T cell clusters are included). Higher expression in myocarditis T cells is indicated by positive fold change. Red indicates FDR-corrected p-value (q-value) <0.05. Black indicates not significant. e) UMAP is subset on only T cells with TCR reads. Clonal is defined as >2 cells with the same TCR clonotype. No clonal cells are seen in the control sample (n=1495 cells). f) The proportion of cells in the naïve or activated T cell clusters are shown stratified by sample and clonality. P-values represent multiple fisher's exact tests. g) Violin plots shown expression of key genes by clonality and sample. Identity genes are shown in light blue. Genes associated with naïve T cells are shown in dark blue. Genes associated with T cell activation are shown in red.

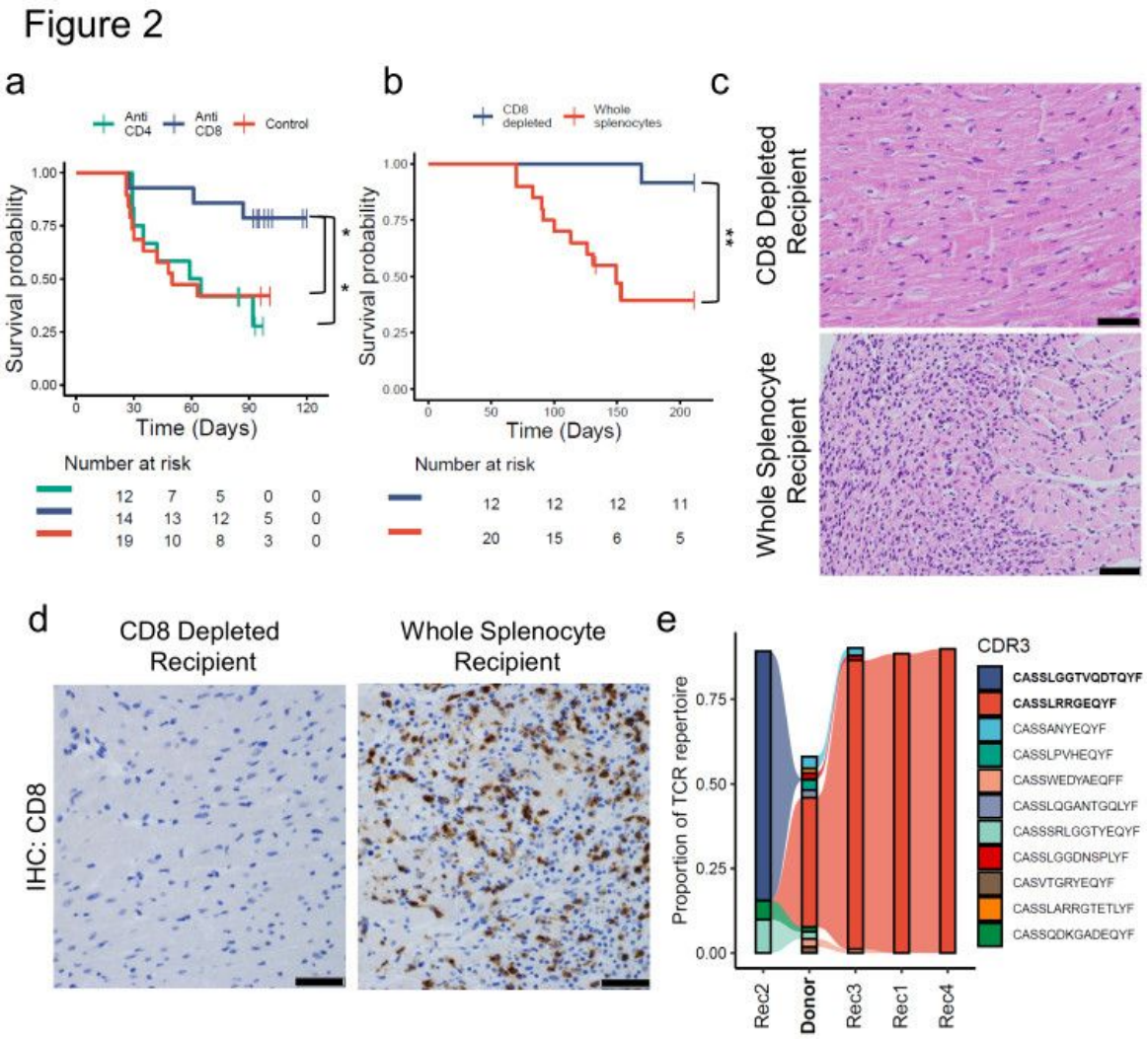

Figure 2

CD8+ T cells are necessary for myocarditis. a) *Pdcd1-/-Ctla4+/-* mice were treated with anti-CD4, anti-CD8 or control antibodies. P-values represent cox proportional hazard tests. Risk tables show size of groups. b) Whole splenocytes or splenocytes from which CD8 cells were depleted from *Pdcd1-/-Ctla4+/-* mice with myocarditis were transferred to *Rag1-/-* recipient mice. P-value represents cox proportional hazard test. Risk tables show size of groups. c) Representative H&E from CD8 depleted splenocyte recipients

compared to whole splenocyte recipients. Only cardiac sections are shown. Scale bars show 50μm. d) Representative IHC for CD8 on cardiac sections from CD8 depleted splenocyte recipients compared to whole splenocyte recipients. Scale bars show 50μm. e) TCR beta chain sequencing on cardiac tissue from a donor *Pdcd1-/-Ctla4+/-* mouse (Donor, in bold) and *Rag1-/-* whole splenocyte recipients (Rec1-4). The top ten most abundant TCRs from the donor plus the most abundant TCR from Rec2 are shown. Flow between samples indicates shared TCRs. Bolded CDR3s indicate most clonal TCRs.

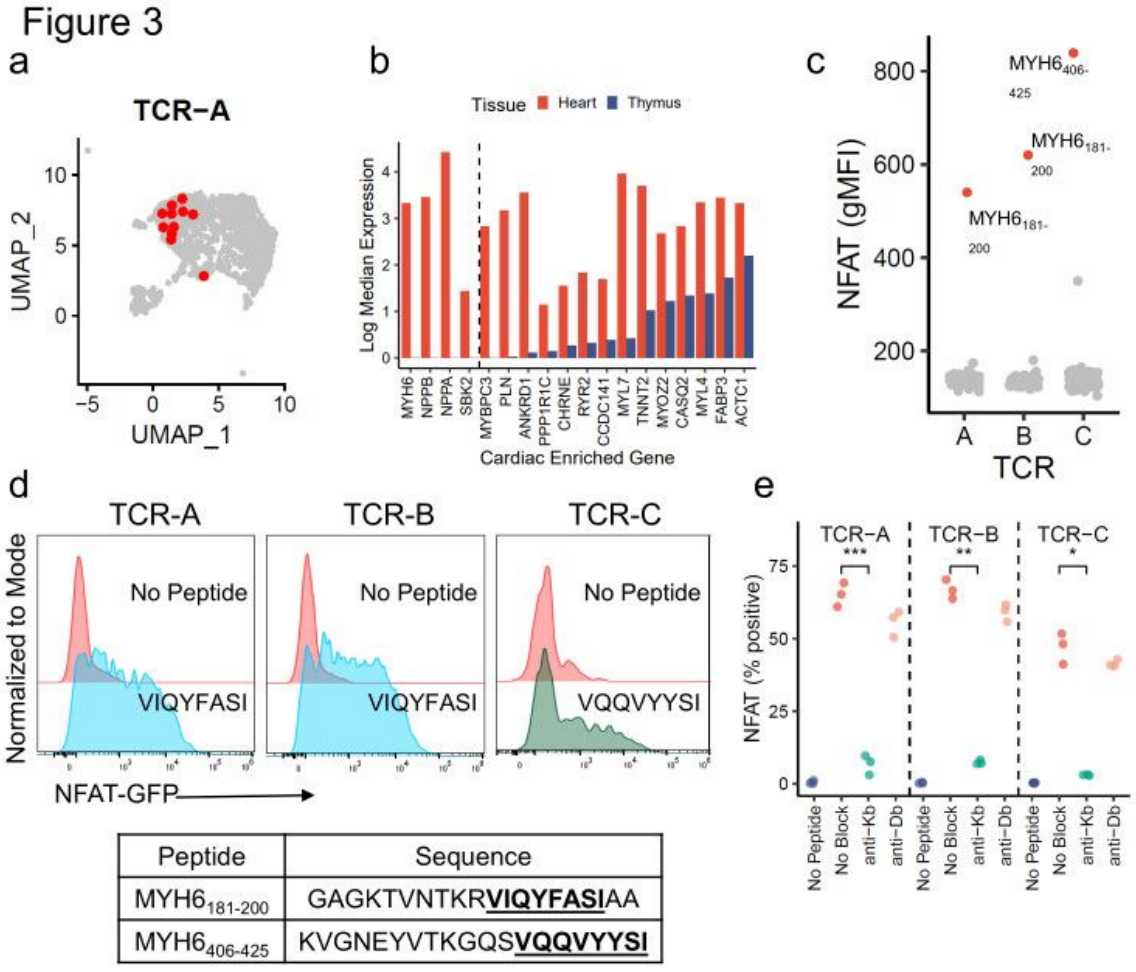

Peptide	Sequence
$MYH6_{181-200}$	GAGKTVNTKR**VIQYFASI**AA
$MYH6_{406-425}$	KVGNEYVTKGQS**VQQVYYSI**

Figure 3

Alpha-myosin is an MHC-I restricted autoantigen in murine myocarditis. a) TCR-A, a TCR used for antigen discovery, is shown on the same UMAP plot as shown in Fig. 1e. Red cells indicate cells expressing TCR-A. b) Log median expression of 18 cardiac enriched genes in the heart (red) and thymus (blue). Genes are sorted by thymic expression. Genes to the left of the dashed line have no detectable expression in thymic APCs. c) NFAT-GFP reporter activity, measured by flow cytometry and shown as geometric mean fluorescence intensity, of three TCR cell lines stimulated independently with 130, 10-20aa alpha-myosin peptides. Top peptide hits are colored in red and labeled. d) Representative flow cytometry histograms of each TCR cell line co-cultured with BMDCs and stimulated with 10μg/mL predicted cognate peptide relative to no peptide. Peptide sequences are shown in the table. e) Each TCR cell line was co-cultured with EL-4 APCs and 10μg/mL cognate peptide (VIQYFASI for TCRs A and B; VQQVYSI for TCR C; except for no peptide controls) with or without 10μg/mL of anti-Kb or anti-Db blocking antibody. NFAT-GFP reporter activity is shown as percent of live cells. n=3 biological replicates. P-values represent t-tests.

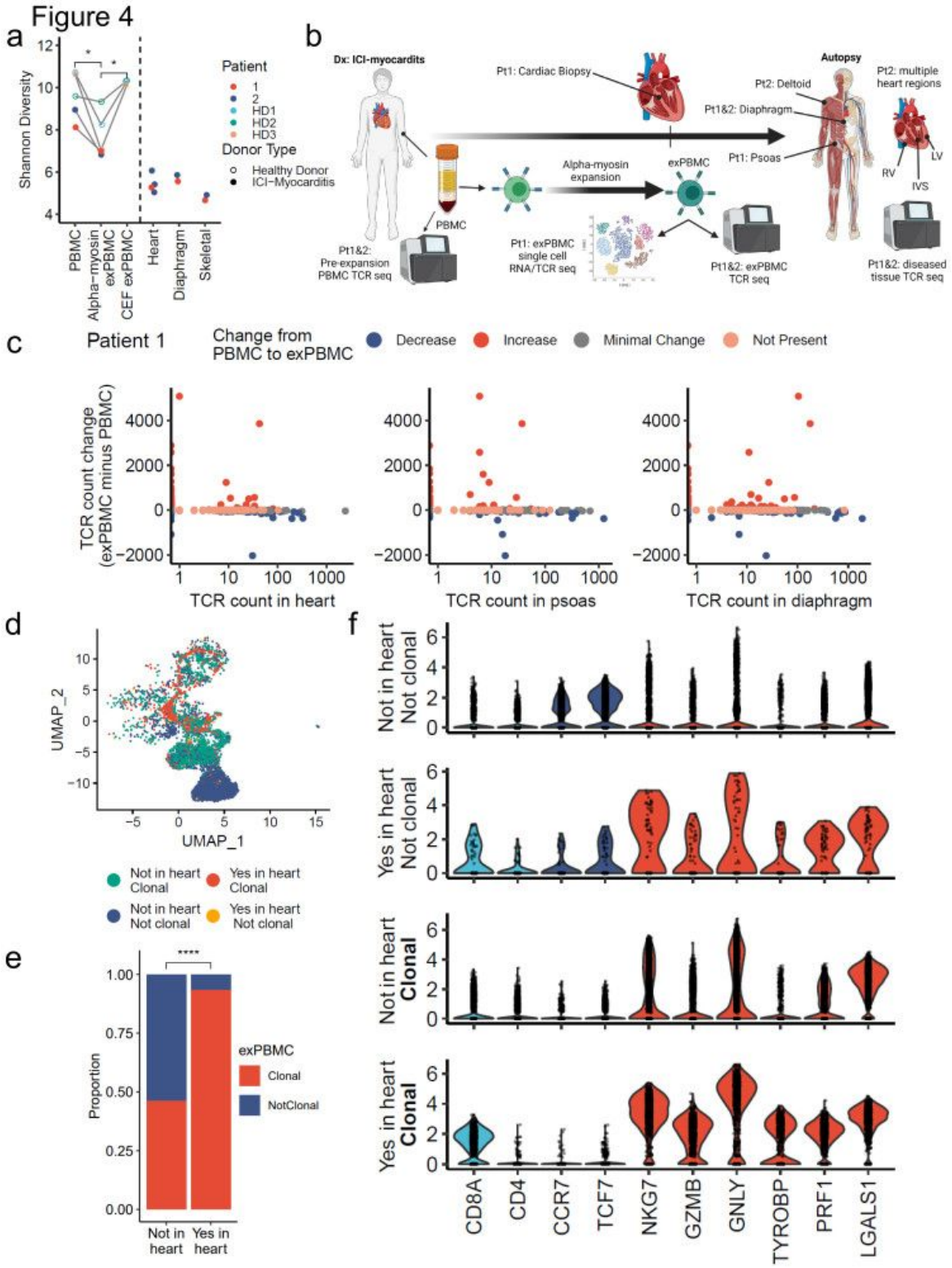

Figure 4

Alpha-myosin expanded TCRs are present in cardiac and skeletal muscle of patients with ICI-myocarditis. a) Shannon diversity of indicated TCR repertoires. Healthy donors are shown in open circles, while myocarditis donors are shown in closed circles. Lines connect the pre-expansion PBMC to the same donor's expanded PBMC (exPBMC). Dashed line separates PBMC and exPBMC from diseased heart and skeletal muscles in myocarditis patients. Skeletal refers to psoas muscle for patient 1 and deltoid muscle

for patient 2. P-values represent t-tests. b) Schematic describing patient tissues and process of expanding PBMCs. RV= right ventricle. LV = left ventricle. IVS = interventricular septum. c) Change in TCR counts from PBMC to alpha-myosin expanded PBMC (exPBMC) plotted by abundance in indicated tissues for patient 1. Minimal change is less than a 50 read count change. Not present means not found in either PBMC or exPBMC, but present in indicated tissue. d) Dimensionality reduction with UMAP on single cell RNA/TCR sequencing of CD3+ sorted patient 1 exPBMC. Only cells with TCR expression are shown. Groups are divided by whether the TCR expressed by that cell is also found in the patient's heart and whether that TCR is clonal (expressed by >2 cells in exPBMC single cell TCR sequencing). d) Proportion of single cell sequenced exPBMCs that are clonal, stratified by whether that TCR is also found in the heart. P<0.0001 by Fisher's Exact test. f) Violin plots of key gene expression by presence or absence in cardiac TCR repertoire and clonality in exPBMC. Identity genes are shown in light blue. Genes associated with naïve T cells are shown in dark blue. Genes associated with T cell activation are shown in red.

Supplementary Files

This is a list of supplementary files associated with this preprint. Click to download.

- SupplementalMaterialTCRsequences.docx
- ExtendedDataTable1.xlsx
- ExtendedDataTable2.xlsx
- ExtendedFigure1.jpg
- ExtendedFigure2.jpg
- ExtendedFigure3.jpg
- ExtendedFigure4.jpg
- ExtendedFigure5.jpg